JOURNAL OF GUIDANCE, CONTROL, AND DYNAMICS
Vol. 33, No. 1, January–February 2010

Optimal Control of Electrodynamic Tether Orbit Transfers Using Timescale Separation

Paul Williams*
Delft University of Technology, 2629 HS Delft, The Netherlands

DOI: 10.2514/1.45250

Electrodynamic tether systems have the potential to allow orbital maneuvers to be undertaken with little or no propellant. However, when operated in this mode, the current must be modulated on a fast timescale compared with the variation in the average orbital elements. This paper introduces a new numerical technique for calculating optimal trajectories for general dynamical systems for which the dynamics evolve on multiple timescales. The method combines quadrature and pseudospectral methods using the Chebyshev–Gauss–Lobatto points, which are shown to be ideal for handling timescale separation. The resulting nonlinear programming problem generates a significantly reduced problem size compared with solving the full-scale problem. Numerical results for a problem with an analytic solution show that the method achieves high accuracy. Results generated for hanging and spinning electrodynamic tethers demonstrate that spinning electrodynamic tethers can be more efficient for orbital maneuvering.

Nomenclature

a = orbit semimajor axis, km
$\mathcal{D}_{k,j}$ = entry of differentiation matrix, row k, column j
e = orbit eccentricity
$\boldsymbol{e}_L^f$ = lower bound on endpoint conditions at final time
$\boldsymbol{e}_U^f$ = upper bound on endpoint conditions at final time
$\boldsymbol{e}_L^0$ = lower bound on endpoint conditions at initial time
$\boldsymbol{e}_U^0$ = upper bound on endpoint conditions at initial time
f_h = normal perturbed acceleration of center of mass, $\mathrm{m/s^2}$
f_r = radial perturbed acceleration of center of mass, $\mathrm{m/s^2}$
f_t = transverse perturbed acceleration of center of mass, $\mathrm{m/s^2}$
$\boldsymbol{f}_{\omega_1}$ = vector field for slow dynamics
$\boldsymbol{f}_{\omega_2}$ = vector field for fast dynamics
h = orbital angular momentum
I = electric current, A
$\mathcal{I}_{j,k}$ = entry of integration matrix, row k, column j
i = orbit inclination, rad
$\mathcal{J}$ = performance index for optimization
L = tether length, m
$\mathcal{L}$ = integrand of the Bolza cost function
m = tether system mass, kg
N_{ω_1} = number of nodes used for discretization of slow time
N_{ω_2} = number of nodes used for discretization of fast time
$\boldsymbol{p}_L$ = lower bound on path constraints
$\boldsymbol{p}_U$ = upper bound on path constraints
p = semilatus rectum, km
r = orbit radius, km
$\boldsymbol{T}_k$ = Chebyshev polynomial of order k
t = physical time
t_f = final time
t_0 = initial time
$\boldsymbol{u}$ = control inputs
$\boldsymbol{x}_{\omega_1}$ = slow-state variable
$\boldsymbol{x}_{\omega_2}$ = fast-state variable
$\mathcal{E}$ = Mayer cost function
θ = in-plane libration angle, rad
μ = gravitation parameter, $\mathrm{m^3/s^2}$
μ_m = dipole strength of Earth's magnetic field
ν = true anomaly, rad
τ = computational domain for Chebyshev polynomials
$\Phi_{k,j}$ = entry of interpolation matrix, row k, column j
ϕ_k = Lagrange interpolating polynomial at kth node
Ω = right ascension of ascending node, rad
ω = argument of perigee, rad

Received 2 May 2009; revision received 27 July 2009; accepted for publication 30 July 2009.

*Researcher; currently at 1/4 Maylands Avenue, Balwyn North Victoria 3104, Australia. Member AIAA.

Introduction

MANY dynamical systems have dynamics that evolve on different timescales. A typical example is a rigid-body aircraft, which has fast dynamics associated with attitude dynamics and slow dynamics associated with the translational motion. It is this fact that is often exploited in control system design, for which an inner and outer loop are employed. The inner loop is designed to stabilize the fast dynamics, whereas the outer loop is designed to control the slower dynamics. Determining numerical optimal trajectories for such systems using direct transcription methods has either been tackled by treating only the slow dynamics [1–3], for which a coarse mesh can be used, or by discretizing the full dynamics, for which a finer mesh or combination of a coarse mesh and repeatedly solving a sequence of problems with moving initial conditions is required [4,5]. Recently, Desai and Conway [6] presented an approach that modified the original approach presented by Herman and Conway [7], which effectively allowed different meshes to be used by the fast and slow dynamics. In the method presented by Desai and Conway [6], the entire time domain is divided into a sequence of smaller intervals in which low-order polynomial approximations are used for the slow states. The same polynomial order is used for the fast states, but each interval is further subdivided into two or four subintervals for approximation of the fast states. This paper develops an alternative approach suitable for solving optimal control problems on multiple timescales. At its core is the Chebyshev pseudospectral method, which uses a Gauss–Lobatto grid and Lagrange interpolating polynomials to approximate the fast states. The slow states are approximated via numerical quadrature, which allows significantly fewer nodes to be used and, thus, results in a smaller problem size.

This paper is motivated by the problem of determining optimal trajectories for electrodynamic tethered systems. When used for modifying the orbital elements of the system center of mass, the set of dynamical equations that govern the evolution of the system have components that exhibit fast and slow motion. For example, the mean

orbital elements vary slowly with time, whereas the current (control) input typically varies at a much faster rate. In [8], Williams determined optimal trajectories for an electrodynamic tether including the effects of tether libration using direct transcription methods. A fine mesh was used for all dynamical states, which results in a very large-scale nonlinear programming problem. Tragesser and San [9] developed a simple approach for controlling the orbital elements of a hanging electrodynamic tether. The approach assumes a fixed form for the current variation, based on a Fourier series expansion. By fixing the average orbital elements, the required coefficients of the current are determined after analytically integrating the orbit perturbation equations based on small eccentricities. To account for limitations on the current draw, it is necessary to scale the time of flight accordingly. Williams [10] adapted this approach for the case of spinning electrodynamic tether systems. Stevens and Wiesel [11] developed the approach further by using modified equinoctial elements and applied the Legendre pseudospectral method to obtain optimal maneuvers for a hanging tether. The approach in [11] optimizes the coefficients of the Fourier series expansion for the current and enforces constraints on the maximum current by limiting the average power. The approach is still limited to small eccentricities, and further application requires rederiving the change in orbital elements due to the electric current. Williams et al. [12] developed a recursive algorithm for solving orbit transfer problems with electrodynamic tethers using direct shooting. The approach is suboptimal for long maneuver times, but has the advantage that it easily accounts for librating and spinning tethers.

This paper makes several contributions in the area of trajectory optimization for electrodynamic orbit transfers. First, an approach for solving general optimal control problems for systems for which a separation of timescales exists in the dynamics is presented. The approach is based on approximating the state and control trajectories using Lagrange interpolating polynomials. The nodes selected for discretizing the problem are the Chebyshev–Gauss–Lobatto (CGL) points, which have properties that prove to be very convenient when dealing with problems involving timescale separation. In contrast to the results in [11], no analytical approximations are required for the approximation of the variation in orbital elements, and no assumption about the variation in electric current is needed. The numerical approach is derived and first applied to a simple problem with an analytic solution. The approach is then applied to the problem of determining optimal orbital transfers of electrodynamic tethers. It will be shown that the approach can accurately determine optimal trajectories for electrodynamic tethers involving both hanging and spinning tethers.

Optimal Control Problems with Timescale Separation

Problem Statement

To facilitate the discussion, a rather general optimal control problem may be considered. Consider the problem of determining the slow-state–fast-state control triple $\{\boldsymbol{x}_{\omega_1}(\cdot), \boldsymbol{x}_{\omega_2}(\cdot), \boldsymbol{u}(\cdot)\}$ so as to minimize the cost function

$$\mathcal{J} = \mathcal{E}[\boldsymbol{x}_{\omega_1}(t_0), \boldsymbol{x}_{\omega_1}(t_f), \boldsymbol{x}_{\omega_2}(t_0), \boldsymbol{x}_{\omega_2}(t_f), t_0, t_f] + \int_{t_0}^{t_f} \mathcal{L}[\boldsymbol{x}_{\omega_1}(t), \boldsymbol{x}_{\omega_2}(t), \boldsymbol{u}(t), t]\,\mathrm{d}t \tag{1}$$

subject to the nonlinear state equations for the slow states

$$\dot{\boldsymbol{x}}_{\omega_1}(t) = \boldsymbol{f}_{\omega_1}(\boldsymbol{x}_{\omega_1}(t), \boldsymbol{x}_{\omega_2}(t), \boldsymbol{u}(t), t) \tag{2}$$

the nonlinear state equations for the fast states

$$\dot{\boldsymbol{x}}_{\omega_2}(t) = \boldsymbol{f}_{\omega_2}(\boldsymbol{x}_{\omega_1}(t), \boldsymbol{x}_{\omega_2}(t), \boldsymbol{u}(t), t) \tag{3}$$

the endpoint conditions

$$\boldsymbol{e}^0_L \le \boldsymbol{e}[\boldsymbol{x}_{\omega_1}(t_0), \boldsymbol{x}_{\omega_2}(t_0), t_0] \le \boldsymbol{e}^0_U \tag{4}$$

$$\boldsymbol{e}^f_L \le \boldsymbol{e}[\boldsymbol{x}_{\omega_1}(t_f), \boldsymbol{x}_{\omega_2}(t_f), t_f] \le \boldsymbol{e}^f_U \tag{5}$$

path constraints

$$\boldsymbol{p}_L \le \boldsymbol{p}[\boldsymbol{x}_{\omega_1}(t), \boldsymbol{x}_{\omega_2}(t), \boldsymbol{u}(t), t] \le \boldsymbol{p}_U \tag{6}$$

and box constraints

$$\begin{aligned} &\boldsymbol{x}_{\omega_1 L} \le \boldsymbol{x}_{\omega_1}(t) \le \boldsymbol{x}_{\omega_1 U} \qquad \boldsymbol{x}_{\omega_2 L} \le \boldsymbol{x}_{\omega_2}(t) \le \boldsymbol{x}_{\omega_2 U} \\ &\boldsymbol{u}_L \le \boldsymbol{u}(t) \le \boldsymbol{u}_U \end{aligned} \tag{7}$$

where $\boldsymbol{x}_{\omega_1} \in \mathbb{R}^{n_x^{\omega_1}}$, $\boldsymbol{x}_{\omega_2} \in \mathbb{R}^{n_x^{\omega_2}}$, $\boldsymbol{u} \in \mathbb{R}^{n_u}$, $t \in \mathbb{R}$, $\mathcal{E}$: $\mathbb{R}^{n_x^{\omega_1}} \times \mathbb{R}^{n_x^{\omega_1}} \times \mathbb{R}^{n_x^{\omega_2}} \times \mathbb{R}^{n_x^{\omega_2}} \times \mathbb{R} \times \mathbb{R} \to \mathbb{R}$, $\mathcal{L}$: $\mathbb{R}^{n_x^{\omega_1}} \times \mathbb{R}^{n_x^{\omega_2}} \times \mathbb{R}^{n_u} \times \mathbb{R} \to \mathbb{R}$, $\boldsymbol{e}^0_L$, $\boldsymbol{e}^0_U \in \mathbb{R}^{n_x^{\omega_1}} \times \mathbb{R}^{n_x^{\omega_2}} \times \mathbb{R} \to \mathbb{R}^{n_0}$, $\boldsymbol{e}^f_L$, $\boldsymbol{e}^f_U \in \mathbb{R}^{n_x^{\omega_1}} \times \mathbb{R}^{n_x^{\omega_2}} \times \mathbb{R} \to \mathbb{R}^{n_f}$, $\boldsymbol{p}_L$, and $\boldsymbol{p}_U \in \mathbb{R}^{n_x^{\omega_1}} \times \mathbb{R}^{n_x^{\omega_2}} \times \mathbb{R}^{n_u} \times \mathbb{R} \to \mathbb{R}^{n_p}$. This optimal control problem is discretized and then solved using nonlinear programming.

This optimal control problem formulation is easily extended to the case of three or more different timescales or the separation of the control inputs to multiple timescales. In this work, however, the control input is assumed to be applied to the fast timescale, t_{ω_2}. It is a trivial extension to consider the control input applied to the slow timescale.

Numerical Solution Approach

Typical approaches for solving optimal control problems of the type described in the previous section include Hermite-based methods [6,7] or higher-order versions [13] and pseudospectral methods [14,15]. The Hermite-interpolating-based approaches approximate the state trajectories using Hermite-interpolating polynomials using a set of basis nodes that coincide with the Legendre–Gauss–Lobatto (LGL) points for a specified polynomial order. Pseudospectral methods approximate the state trajectories using Nth-order Lagrange interpolating polynomials and typically use the LGL points as the nodes, although the Jacobi–Gauss–Lobatto points are the most general set of classical nodes [16]. The LGL points are the natural set of points to use for approximating boundary value problems because they are formulated to integrate polynomial functions exactly for degrees up to $2N - 1$. The CGL points have also been used for solving optimal control problems [17,18] and have the advantage that the locations of the nodes have a closed-form solution.

In all the aforementioned techniques, the goal is to convert the continuous optimal control problem into a discrete parameter optimization problem that can be solved using standard nonlinear programming software. This paper follows this same approach, but proposes a different means for approximating the multiple-timescale states problem. The key idea of this paper is to employ different discretizations for the slow- and fast-state variables. The fast variables are discretized by means of a differentiation approach, whereas the slow variables are discretized by means of a quadrature approach. The discretizations are unified by choice of nodes, as elaborated in the following subsection.

Node Selection

The principle idea of this work is that the slowly varying states do not need to be discretized using the same number of nodes as the faster states. At the same time, it is desirable to capture the effects of the variations in fast states and the control inputs on the slow states. It is possible to combine these two properties by exploiting some key properties of pseudospectral methods, namely, node selection and quadrature.

For boundary value problems, the Gauss–Lobatto points are a natural choice for nodes because they combine a high accuracy of interpolation with highly accurate quadrature approximations. Two popular choices for Gauss–Lobatto points have been used widely in the literature. Legendre–Gauss–Lobatto and Chebyshev–Gauss–Lobatto points are based on the roots of the derivatives of Legendre and Chebyshev polynomials, respectively, which are two instances of the more general Jacobi polynomials. The LGL points minimize

the L_2 norm of the approximation error, whereas the CGL points minimize the maximum norm of the approximation error. When N nodes are used, the LGL quadrature rule is exact for polynomials of the order $2N-1$, whereas when the CGL points are used, the corresponding Curtis–Clenshaw quadrature rule is only exact for polynomials of order N. However, the CGL points have an important property that is useful for implementing a multiple-to-one timescale collocation approach. To understand this point, consider the CGL nodes for an Nth order polynomial defined over the interval $\tau \in [-1, 1]$:

$$\tau_j = -\cos\left(\frac{\pi j}{N}\right), \qquad j = 0, \ldots, N \tag{8}$$

For any base number of nodes N_{ω_1} and base 2 multiplier i, the jth node corresponds to the $2^i j$th node because

$$\tau^{\omega_2}_{2^i j} = -\cos\left(\frac{\pi 2^i j}{2^i N_{\omega_1}}\right) = \tau^{\omega_1}_j \tag{9}$$

where the superscript ω_1 denotes the slow time base, and ω_2 denotes the fast time. The advantage in this for multiple-to-one timescale collocation is that no interpolation of the high-frequency states is required. The slower states will have collocation points that correspond exactly with a subset of the faster states. This is illustrated in Fig. 1, which shows the set of nodes for $N = 10$, 20, and 30. In this figure, $N = 10$ represents the nodes corresponding to the discretization of the slow states. For a two-to-one discretization of the fast states, $N = 20$, the fast states are discretized with an additional node between the slow-state nodes. For a three-to-one discretization of the fast states, $N = 30$, the fast states have three additional nodes between the slow-state nodes. Arbitrary multiple-to-one discretizations are possible using this approach. Hence, the slow-state nodes always coincide with a subset of the faster nodes.

State and Control Approximations

Fast States

The approximation of the fast states is performed using a standard Chebyshev pseudospectral method [18], with the difference that the derivatives of the vector field are a function of the fast and slow states. The fast states and controls are approximated using N_{ω_2}th degree Lagrange interpolating polynomials:

$$\boldsymbol{x}_{\omega_2}(\tau) = \sum_{k=0}^{N_{\omega_2}} (\boldsymbol{x}_{\omega_2})_k \phi_k(\tau), \qquad \boldsymbol{u}(\tau) = \sum_{k=0}^{N_{\omega_2}} (\boldsymbol{u})_k \phi_k(\tau) \tag{10}$$

where

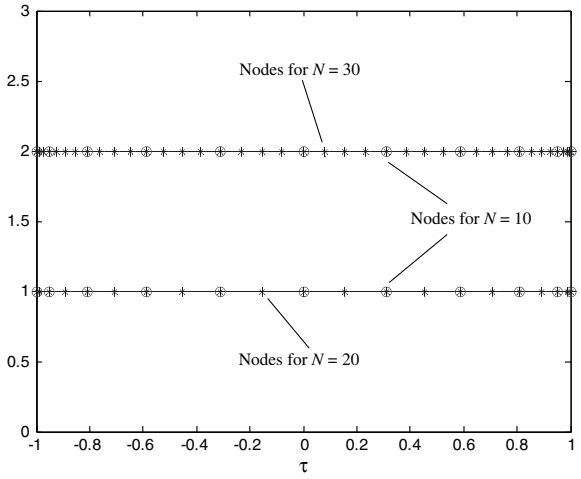

Fig. 1 Examples of node distributions using Chebyshev–Gauss–Lobatto points.

$$\phi_k(\tau) = \prod_{\substack{j=0 \\ j\neq k}}^{N_{\omega_2}} \left(\frac{\tau - \tau_j}{\tau_k - \tau_j}\right) = \frac{g(\tau)}{(\tau - \tau_k) g'(\tau_k)}, \qquad k = 0, \ldots, N_{\omega_2} \tag{11}$$

is the general form of the Lagrange interpolating polynomial with nodes at τ_k, and $(\boldsymbol{x}_{\omega_2})_k$ and $(\boldsymbol{u})_k$ are the values of the fast states and controls at the nodes τ_k. For the CGL nodes, Eq. (11) can be expressed in terms of the N_{ω_2}th degree Chebyshev polynomial $T_{N_{\omega_2}}(\tau)$ as follows:

$$\phi_k(\tau) = \frac{(-1)^{k+1}(1-\tau^2) T'_{N_{\omega_2}}(\tau)}{c_k N_{\omega_2}(\tau - \tau_k)}, \qquad k = 0, \ldots, N_{\omega_2} \tag{12}$$

where

$$c_k = \begin{cases} 2 & k = 0, N_{\omega_2} \\ 1 & 1 \le k \le N_{\omega_2} \end{cases} \tag{13}$$

The Chebyshev polynomials of order k are defined as follows:

$$T_k(\tau) = \cos(k \cos^{-1}(\tau)), \qquad \tau \in [-1, 1] \tag{14}$$

The fast states are approximated using the standard Chebyshev pseudospectral method, which differentiates the approximating polynomial for the state trajectory and forces it to be equal to the state equations at the CGL nodes. Derivatives of the state vector at the CGL points may be related to the state vector at the CGL points by way of a differentiation matrix:

$$\boldsymbol{x}'_{N_{\omega_2}}(\tau_k) = \sum_{j=0}^{N_{\omega_2}} (\boldsymbol{x}_{\omega_2})_j \phi'_j(\tau_k) = \sum_{j=0}^{N_{\omega_2}} \mathcal{D}_{k,j} (\boldsymbol{x}_{\omega_2})_j \tag{15}$$

where the coefficients $\mathcal{D}_{k,j}$ are entries of a $(N_{\omega_2}+1) \times (N_{\omega_2}+1)$ differentiation matrix, $\boldsymbol{\mathcal{D}}$:

$$\begin{aligned} \boldsymbol{\mathcal{D}} &:= [\mathcal{D}_{k,j}] \\ &= \begin{cases} (c_k/c_j)[(-1)^{j+k}/(\tau_k - \tau_j)], & j \neq k \\ -\tau_k/[2(1-\tau_k^2)], & 1 \le j = k \le N-1 \\ -(2N^2+1)/6, & j = k = 0 \\ (2N^2+1)/6, & j = k = N \end{cases} \end{aligned} \tag{16}$$

The computational domain for the CGL nodes is $\tau \in [-1, 1]$, whereas the physical time domain is $t \in [t_0, t_f]$. The computation domain is mapped to the physical domain via

$$t = \frac{t_f - t_0}{2}\tau + \frac{t_f + t_0}{2} \tag{17}$$

Using this definition, the state equations are enforced using equality constraints of the form

$$\frac{2}{t_f - t_0} \sum_{j=0}^{N_{\omega_2}} \mathcal{D}_{k,j} (\hat{\boldsymbol{x}}_{\omega_2})_j - \boldsymbol{f}_{\omega_2}(\boldsymbol{x}_{\omega_1}, \boldsymbol{x}_{\omega_2}, \boldsymbol{u}, t)|_{t_k} = 0$$
$$k = 0, \ldots, N_{\omega_2} \tag{18}$$

The slow states that appear in Eq. (18) are not known explicitly at all the CGL nodes corresponding to the fast states. Instead, the slow states must be interpolated at the fast nodes. This is achieved by way of the Lagrange polynomial on which the approximations are based. For implementation, the interpolated slow states are obtained via a matrix–vector product as follows

$$\boldsymbol{x}_{\omega_1}(\tau_{\omega_2}) = \boldsymbol{\Phi} \boldsymbol{x}_{\omega_1}(\tau_{\omega_1}) \tag{19}$$

where the entries of the $(N_{\omega_2}+1) \times (N_{\omega_1}+1)$ interpolation matrix $\boldsymbol{\Phi}$ are given by

$$\Phi_{k,j} = \begin{cases} \dfrac{(-1)^{j+1}(1-\tau_k^2)T'_{N_{\omega_2}}(\tau_k)}{c_j N_{\omega_2}(\tau_k - \tau_j)}, & k \neq j, j = 0, \ldots, N_{\omega_2} \\ 1, & k = j \end{cases} \tag{20}$$

Slow States

The differentiation approach used in the pseudospectral method is not suitable for discretizing the slow dynamics because it would ignore the variation in the fast states and/or control between the slow nodes. That is, the differentiation approach enforces the dynamics in an approximate fashion by forcing the derivative of the approximating polynomial to be equal to the vector field at the nodes in a pointwise fashion. To accumulate the information of the fast state in the average slow state, the use of integration rather than differentiation is the natural choice. The slow states are enforced by using quadrature constraints in a similar manner to that used by Williams [19] and Williams and Trivailo [20]. In [20], integration of the states was performed analytically for the case of $N = 5$, whereas Williams [19] derived a general integration matrix for an arbitrary number of nodes. In [19,20], the LGL nodes were used and only the case of a single timescale was considered. In this section, quadrature constraints are derived for the case of multiple timescales using the CGL nodes.

For the variation in the slow state to account for the fast-state information, the vector field of the slow state must be discretized at the fast nodes and not just at the slow nodes. To achieve this, the vector field is approximated directly by means of N_{ω_2}th degree Lagrange interpolating polynomials:

$$\boldsymbol{f}_{\omega_1}(\tau) = \sum_{k=0}^{N_{\omega_2}} (\boldsymbol{f}_{\omega_1})_k \phi_k(\tau) \tag{21}$$

Because the values of the vector field at the fast CGL nodes are used in Eq. (21), the values of the states and controls at the fast CGL nodes appear directly in the evaluation of Eq. (21). Note the difference in subscript corresponding to the fast nodes and the approximation of the vector field of the slow states at the fast nodes. Integration of Eq. (21) from t_0 to the slow node times leads to

$$(\boldsymbol{x}_{\omega_1})_j = (\boldsymbol{x}_{\omega_1})_0 + \left(\frac{t_f - t_0}{2}\right) \int_{-1}^{\tau_j} \sum_{k=0}^{N_{\omega_2}} \phi_k(\tau)(\boldsymbol{f}_{\omega_1})_k \, \mathrm{d}\tau \qquad j = 1, \ldots, N_{\omega_1} \tag{22}$$

If we define the integral of the Lagrange interpolating polynomials to be the entries of a $N_{\omega_1} \times (N_{\omega_2} + 1)$ integration matrix

$$\mathcal{I}_{j-1,k} \triangleq \int_{-1}^{\tau_j} \phi_k(\tau) \, \mathrm{d}\tau, \qquad j = 1, \ldots, N_{\omega_1}; \qquad k = 0, \ldots, N_{\omega_2} \tag{23}$$

then the discrete constraints for the slow states can be written in the form of a matrix multiplication:

$$(\boldsymbol{x}_{\omega_1})_j = (\boldsymbol{x}_{\omega_1})_0 + \left(\frac{t_f - t_0}{2}\right) \sum_{k=0}^{N_{\omega_2}} \mathcal{I}_{j-1,k} (\boldsymbol{f}_{\omega_1})_k, \qquad j = 1, \ldots, N_{\omega_1} \tag{24}$$

The entries of the integration matrix may be calculated from the following closed-form solution (see the Appendix for a derivation):

$$\mathcal{I}_{j-1,k} = \frac{1}{[T'_{N+1}(\tau_k) - T'_{N-1}(\tau_k)]T_N(\tau_k)} \left[T_N(\tau_k) \int_{-1}^{\tau_j} T_N(\tau) \, \mathrm{d}\tau + 2 \sum_{p=0}^{N-1} T_p(\tau_k) \int_{-1}^{\tau_j} T_p(\tau) \, \mathrm{d}\tau \right] \tag{25}$$

with

$$\int_{-1}^{\tau_j} T_p(\tau) \, \mathrm{d}\tau = \frac{1}{2} \left[\frac{T_{p+1}(\tau)}{p+1} - \frac{T_{p-1}(\tau)}{p-1} \right]_{-1}^{\tau_j} \tag{26}$$

The slow-state dynamics are enforced by using Eq. (24) as a nonlinear equality constraint in the nonlinear programming problem.

Performance Index

The integral performance index is discretized via a quadrature rule across the entire time interval. Using the interpolation matrix, the slow states are interpolated at the fast-node times. Hence, all states and control values are obtained at the fast-node times. The integral performance index is then approximated using the following quadrature rule:

$$\int_{t_0}^{t_f} \mathcal{L}[\boldsymbol{x}_{\omega_1}(t), \boldsymbol{x}_{\omega_2}(t), \boldsymbol{u}(t), t] \, \mathrm{d}t \approx \left(\frac{t_f - t_0}{2}\right) \sum_{k=0}^{N_{\omega_2}} \mathcal{I}_{N_{\omega_1}-1,k} \mathcal{L}[\boldsymbol{x}_{\omega_1}(t_k), \boldsymbol{x}_{\omega_2}(t_k), \boldsymbol{u}(t_k), t_k] \tag{27}$$

Note that the last row of the integration matrix is an alternative representation of the Clenshaw–Curtis quadrature rule.

Sparsity

The solution speed of most nonlinear programming software is significantly enhanced if the Jacobian of the nonlinear constraints is sparse in nature, that is, the majority of nonzero terms appear along or close to the diagonal. The sparsity of the Jacobian can be increased by dividing the entire time interval into a series of subdomains and applying the discretization to each subdomain. Continuity of states is achieved by means of enforcing link conditions between each subdomain. Ross and Fahroo generalized this idea to consider various types of link conditions called knots in [21]. It should be noted that the discretization developed in this paper can be applied to more advanced knotting conditions. However, the approach adopted in this paper is to simply divide the entire time interval into M equal subintervals, with the states linked across the subintervals via equality constraints.

Summary of Algorithm

The implementation of the transcription algorithm is summarized using the following key steps:

1) Choose a level of discretization for the slow states, N_{ω_1}.

2) Choose an integer multiple of the slow state, n, for discretization of the fast states and control inputs, $N_{\omega_2} = nN_{\omega_1}$.

3) Obtain the node distributions for the slow and fast states using Eq. (8).

4) Form the interpolation matrix using Eq. (20).

5) Form the differentiation matrix using Eq. (16).

6) Form the integration matrix using Eq. (25).

7) Discretize the state dynamics, cost function, boundary conditions, and link conditions using Eqs. (18), (24), and (27). The equations for the boundary and link conditions are trivial.

8) Solve the resulting nonlinear programming problem using large-scale optimization software, for example, SNOPT [22].

Analytic Example

To demonstrate the applicability of the discretization approach, a simple optimal control problem is considered with an analytic solution. Consider the problem of minimizing the cost function

$$\mathcal{J} = \int_0^{t_f} \frac{1}{2} u^2 \, \mathrm{d}t \tag{28}$$

subject to the state equations

$$\dot{x}_1 = x_2 \tag{29}$$

$$\dot{x}_2 = C\sin(kt) + u \tag{30}$$

together with the endpoint constraints

$$x_1(0) = 0, \qquad x_2(0) = 0 \qquad x_1(t_f) = B, \qquad x_2(t_f) = 0 \tag{31}$$

The analytic solution to this problem can be obtained using Pontryagin's maximum principle and is given by

$$\begin{aligned} x_1 &= -(C/k^2)\sin(kt) + c_1(t^3/6) + c_2(t^2/2) + (C/k)t \\ x_2 &= -(C/k)\cos(kt) + c_1(t^2/2) + c_2 t + (C/k) \\ u &= -c_1 t - c_2 \end{aligned} \tag{32}$$

where the constants of integration are given by

$$\begin{aligned} c_1 &= -(6/t_f^2)((C/k)\cos(kt_f) - (C/k) \\ &\quad + (12/t_f^3)(B + (C/k^2)\sin(kt_f) - (C/k)t_f) \\ c_2 &= (2/t_f)((C/k)\cos(kt_f) \\ &\quad - (C/k)) - (6/t_f^2)(B + (C/k^2)\sin(kt_f) - (C/k)t_f) \end{aligned} \tag{33}$$

In this example, the state x_2 is the fast state and x_1 is the slow state if k is chosen to be sufficiently large. If $k \gg C$, then the response of x_1 is dominated by the polynomial variation with respect to time, and the periodic response will have a negligible component. The periodic component in the response of x_2, on the other hand, will have a factor of k greater influence, with a reduced polynomial component.

Figure 2 shows the results obtained from the multiple-timescale pseudospectral method using $N_{\omega_1} = 10$, with an 8:1 scale for the fast states. The constants employed in the solution are $C = 0.1$, $k = 8$, $t_f = 10$, and $B = 1$. The maximum error from the true solution for x_1 is 2.26e − 5 and for x_2 is 8.6e − 6. Note that the exact solution does not have an exact polynomial representation due to the presence of the periodic terms. Hence, the polynomial approximations used in the method do not result in exact solutions. For this particular example, a high number of nodes is needed to capture the variation in the fast state, whereas only a few nodes are needed to capture the variation in the slow state. The difference in the number of decision variables between solving a full-scale pseudospectral discretization and using the multiple-timescale approach for this particular problem approaches 33% as the ratio of fast variables to slow variables grows. For larger-scale problems that involve more state variables, the difference becomes quite significant.

Application to Electrodynamic Tether System

The discretization approach derived in the previous section is applied to the problem of determining optimal orbit transfers for electrodynamic tethers. For simplicity, the tether system is assumed to consist of an inelastic straight tether (constant length) connected to two satellites, modeled as point masses. Because the maximum current allowed to flow through the tether is a function of the local ionospheric plasma density and some other properties of the system, the electric current used for propulsion is typically restricted to small levels. The low magnitude of the electromagnetic forces means that the orbital elements change very slowly; hence, it is more convenient to express the motion of the system using orbital perturbation equations. A set of classical orbital parameters are used in this paper rather than a set of modified equinoctial elements. The approach is easily extended to consider other representations of the orbital elements.

The system model is illustrated in Fig. 3. The motion of the tether system center of mass is governed by the set of general perturbation equations. In Gauss's form, they are

$$\dot{a} = (2a^2/h)[e\sin(\nu)f_r + (p/r)f_t] \tag{34}$$

$$\dot{e} = (1/h)\{p\sin(\nu)f_r + [(p+r)\cos(\nu) + re]f_t\} \tag{35}$$

$$\begin{aligned} \dot{\omega} &= (1/he)[-p\cos(\nu)f_r + (p+r)\sin(\nu)f_t] \\ &\quad - (r\sin(\omega+\nu)\cos i/h\sin i)f_h \end{aligned} \tag{36}$$

$$\dot{i} = (r\cos(\omega+\nu)/h)f_h \tag{37}$$

$$\dot{\Omega} = (r\sin(\omega+\nu)/h\sin i)f_h \tag{38}$$

$$\dot{\nu} = h/r^2 + (1/eh)[p\cos(\nu)f_r - (p+r)\sin(\nu)f_t] \tag{39}$$

where a is the orbit semimajor axis, $h = \sqrt{\mu a(1-e^2)}$ is the orbit angular momentum, ν is the orbit true anomaly, ω is the argument of perigee, $p = a(1-e^2)$ is the semilatus rectum, r is the orbit radius, e is the orbit eccentricity, Ω is the right ascension of the ascending node, i is the orbit inclination, and f_r, f_t, and f_h are the components of the disturbing acceleration vector in the radial, transverse, and orbit normal directions, respectively.

In addition to the orbital elements describing the position of the center of mass of the system, the orientation of the tether is described by the in-plane libration angle, θ. The variation in electrodynamic forces with the in-plane angle is described in the following subsection. The out-of-plane motion is neglected in this paper, which is approximately true for spinning tether systems [12] or for equal satellite masses on the tether tips.

The electromagnetic force acting on an element of the tether is given by the Lorentz equation

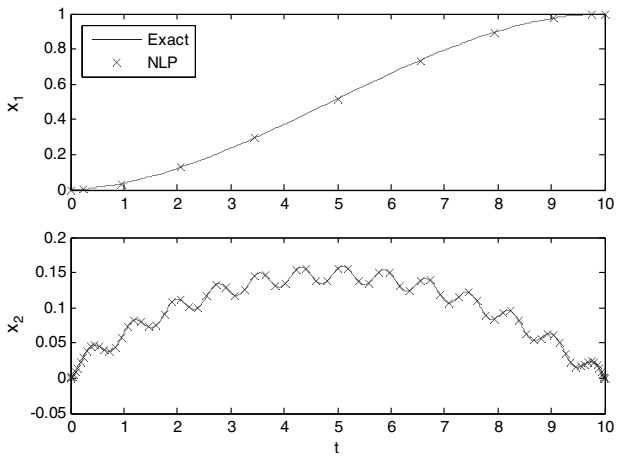

Fig. 2 Comparison of multiple-timescale pseudospectral method with analytical optimal solution using an 8:1 discretization.

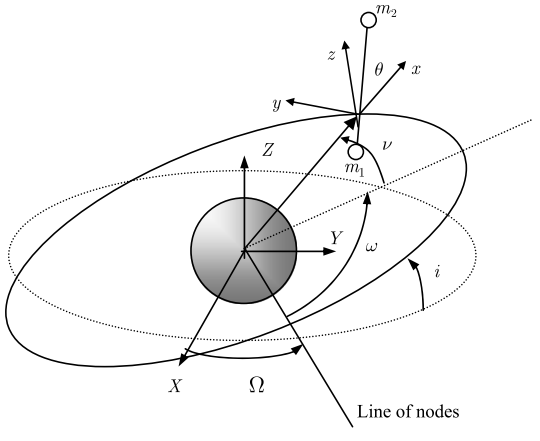

Fig. 3 Simplified electrodynamic tether model.

$$\mathrm{d}\boldsymbol{F} = I\mathrm{d}\boldsymbol{L} \times \boldsymbol{B} \tag{40}$$

where $\mathrm{d}\boldsymbol{L}$ is a vector along the tether line, I is the current in the tether, and $\boldsymbol{B}$ is the magnetic field vector in the orbital frame for which the components are defined by (assuming a nontilted dipole) [23]

$$B_x = -2(\mu_m/r^3)\sin(\omega+\nu)\sin i \tag{41}$$

$$B_y = (\mu_m/r^3)\cos(\omega+\nu)\sin i \tag{42}$$

$$B_z = (\mu_m/r^3)\cos i \tag{43}$$

The electromagnetic forces and torques acting on the system are determined by integrating Eq. (40) along the tether. The resulting perturbative accelerations due to electromagnetic forces are given by

$$f_r = (IL/m)B_z \sin\theta \tag{44}$$

$$f_t = -(IL/m)B_z \cos\theta \tag{45}$$

$$f_h = (IL/m)(B_y \cos\theta - B_x \sin\theta) \tag{46}$$

Note that it has been assumed that a uniform current is flowing through the tether.

Numerical Results

Optimal orbit transfers using electrodynamic tethers have been previously determined using two different approaches. In the first approach used in [8], the entire state trajectory was discretized, and the electric current was determined subject to hard bounds. In the second approach, used in [9–11], the electric current was expanded using a Fourier series with the coefficients of the series selected to be functions of time. The dynamical constraints were enforced using averaged orbital elements. The approach adopted here combines the best of both approaches, in that the electric current is discretized directly, but the slowly varying orbital elements are averaged using numerical integration. Thus, no assumptions about the magnitudes of variables or series expansions are required to carry out the optimizations. It is noted that the approach developed here can be applied purely using the slow-state representation for the states and using the Fourier series form of the control. The problem with using such an approach is that the electric current variation is suboptimal due to the inability to apply hard constraints on the maximum and minimum current.

Short Transfer with Spinning Electrodynamic Tether

The first example serves to illustrate the accuracy of the approach compared with a high-order solution obtained using the Hermite–Simpson method. The Hermite–Simpson method is implemented with 300 equally spaced nodes. The example uses a spinning tether system, in which the spin rate of the tether is assumed to be constant. This contrasts sharply with earlier work that neglects the in-plane librations or rotations of the tether completely. The in-plane angle of the tether is prescribed to be $\theta = 2\nu$. The discretization uses seven subintervals with 20 nodes representing the slow-state solution. Thus, the discretization uses less than half of the nodes of the full solution.

A short orbit transfer is used for comparing the results of the new discretization with that of the Hermite–Simpson method. The problem is to maximize the orbit semimajor axis in a fixed period of time. The other orbit parameters are to remain constant (i.e., return to their original values, except for the semimajor axis) and are given by (initial values)

$$a = 6878 \text{ km}, \quad e = 0.02, \quad \omega = 30 \text{ deg}, \quad i = 30 \text{ deg}, \quad \Omega = 50 \text{ deg}, \quad \nu = 0 \tag{47}$$

The tether length is 15 km, and the total system mass is 420 kg. The current is limited to 4 A and can be backdriven. These are similar values to those used in [8]. Numerical results are shown in Figs. 4 and 5, which show the variation in the orbit semimajor axis and eccentricity for five orbits. Note that the time is nondimensionalized using the mean anomaly corresponding to a circular orbit at the original semimajor axis. Figure 4 shows that the semimajor axis increases by approximately 50 km. There is very good agreement between the high-order discretization and the slow-state approximation. Figure 5 shows the variation in the eccentricity, showing that the slow-state approximation is able to adequately capture the variation in the state. Figure 6 gives the applied current required to achieve the orbital boost, showing the nonperiodic, bang–bang nature of the controls.

Minimum Time Orbit Boost with Hanging Tether

A minimum time orbital boost using a hanging tether was determined using the multiple-scale pseudospectral method. The problem is to maneuver the electrodynamic tether system defined in the previous section from the starting orbit

$$a = 6878 \text{ km}, \quad e = 0.02, \quad \omega = 30 \text{ deg}, \quad i = 30 \text{ deg}, \quad \Omega = 50 \text{ deg}, \quad \nu = 0 \tag{48}$$

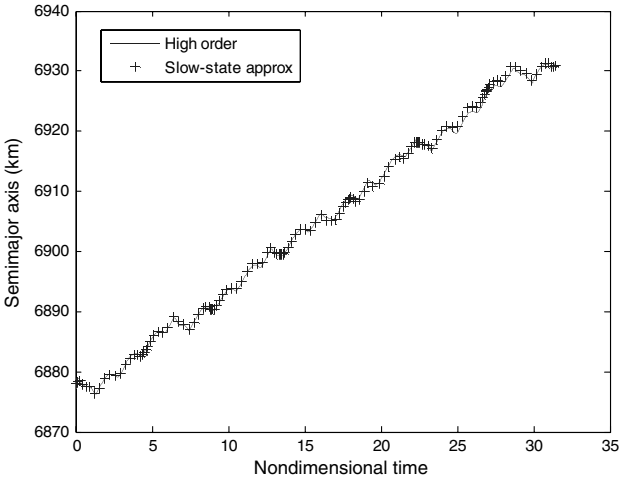

Fig. 4 Comparison of semimajor axis during short orbit transfer with spinning tether, showing 300-node Hermite–Simpson solution with 147-node slow-state solution and 3:1 mapping of control.

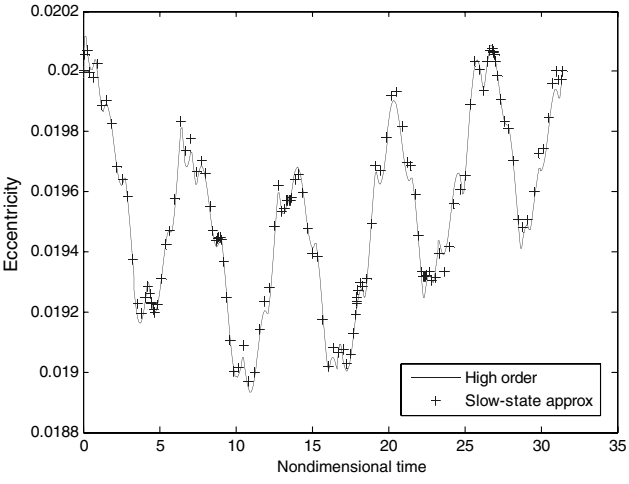

Fig. 5 Comparison of orbit eccentricity during short orbit transfer with spinning tether, showing 300-node Hermite–Simpson solution with 147-node slow-state solution and 3:1 mapping of control.

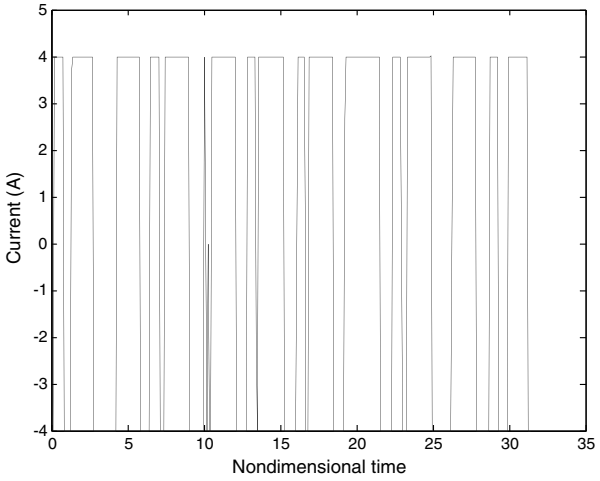

Fig. 6 Applied current for short orbit boost.

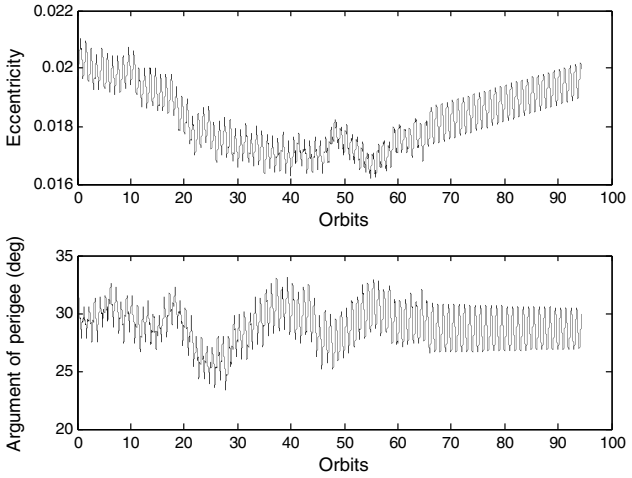

Fig. 8 Orbit eccentricity and argument of perigee during minimum time orbit boost with hanging tether, showing propagated solutions.

to the final orbit

$$a = 8000 \text{ km}, \qquad e = 0.02, \qquad \omega = 30 \text{ deg}, \qquad i = 30 \text{ deg}$$
$$\Omega = 50 \text{ deg} \tag{49}$$

in minimum time. Note that the electric current is assumed to be available at full strength, and no modeling of the variation of the maximum current with ionospheric conditions has been implemented. This assumption should be removed in future work.

The problem was solved using a 3:1 discretization, with $N_{\omega_1} = 20$, and the time domain divided into 30 subintervals. The minimum time for the maneuver was found to be 94.38 orbits. Figure 7 shows the variation in the semimajor axis during the maneuver, Fig. 8 shows the eccentricity and argument of perigee, and Fig. 9 shows the inclination and right ascension of the ascending node. All the solutions shown are the propagated solutions using a Runge–Kutta method with interpolation of the discrete current. These results show that the minimum time maneuver first reduces altitude before climbing. During the descent, the inclination is increased while the ascending node is held approximately constant. The descent is used to speed up the ascent later in the maneuver. The current input is shown in Fig. 10. Initially, the current is applied in a bang–bang manner, but after approximately 60 orbits the current is applied at a constant level of −4 A. This illustrates that the optimal current is not periodic for long maneuver times. The results also show that the method is accurate when propagated using a high-order, small-time-step propagation method.

Minimum Time Inclination Change with Hanging Tether

A minimum time inclination change using a hanging tether was determined using the multiple-scale pseudospectral method. The problem is to maneuver the electrodynamic tether system defined in the previous section from the starting orbit

$$a = 6878 \text{ km}, \qquad e = 0.02, \qquad \omega = 30 \text{ deg}, \qquad i = 30 \text{ deg}$$
$$\Omega = 50 \text{ deg}, \qquad \nu = 0 \tag{50}$$

to the final orbit

$$a = 6878 \text{ km}, \qquad e = 0.02, \qquad \omega = 30 \text{ deg}, \qquad i = 33 \text{ deg}$$
$$\Omega = 50 \text{ deg} \tag{51}$$

in minimum time. This represents an increase in the inclination of 3 deg. The problem was solved using a 3:1 discretization, with $N_{\omega_1} = 20$, and the time domain divided into 30 subintervals. The minimum time for the maneuver was found to be 119.96 orbits. Figure 11 shows the variation in the semimajor axis during the maneuver, Fig. 12 shows the eccentricity and argument of perigee, and Fig. 13 shows the inclination and right ascension of the ascending node. The results illustrate that the inclination increases in a linear fashion, with the system maintaining a slightly lower orbit

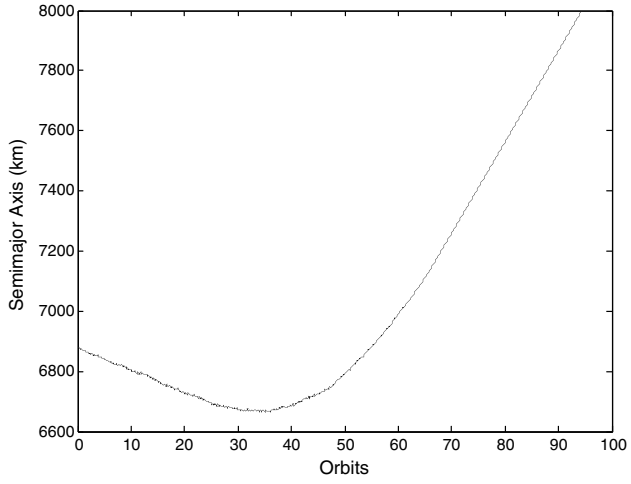

Fig. 7 Orbit semimajor axis during minimum time orbit boost with hanging tether, showing propagated solution.

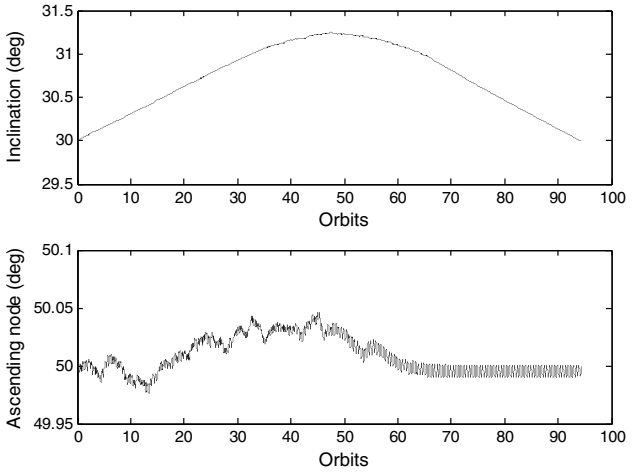

Fig. 9 Orbit inclination and right ascension of ascending node during minimum time orbit boost with hanging tether, showing propagated solutions.

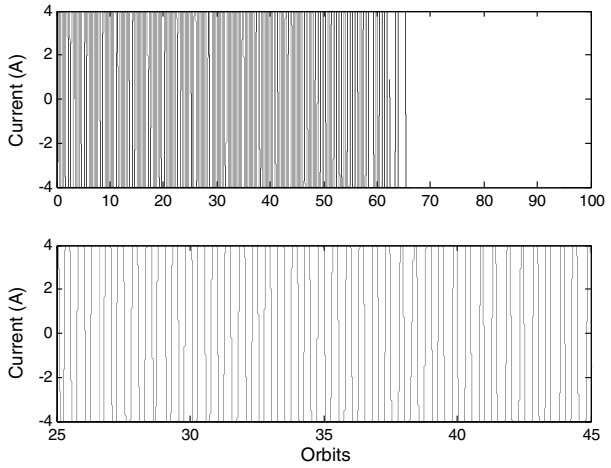

Fig. 10 Electric current during minimum time orbit boost with hanging tether: a) current over whole maneuver, and b) close-up of current between orbits 25 and 45.

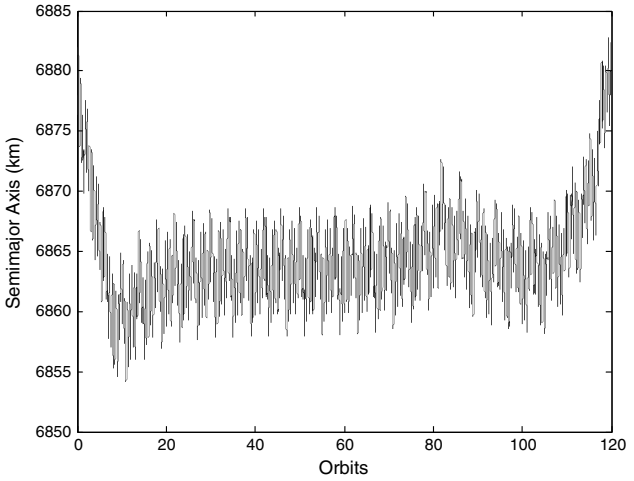

Fig. 11 Orbit semimajor axis during minimum time inclination change with hanging tether, showing propagated solution.

than the original. The electric current is entirely bang–bang throughout the maneuver. The propagated solutions show that the method is accurate and captures the changes in the states due to the bang–bang control quite well. The variation of the orbital elements is not secular over long periods of time.

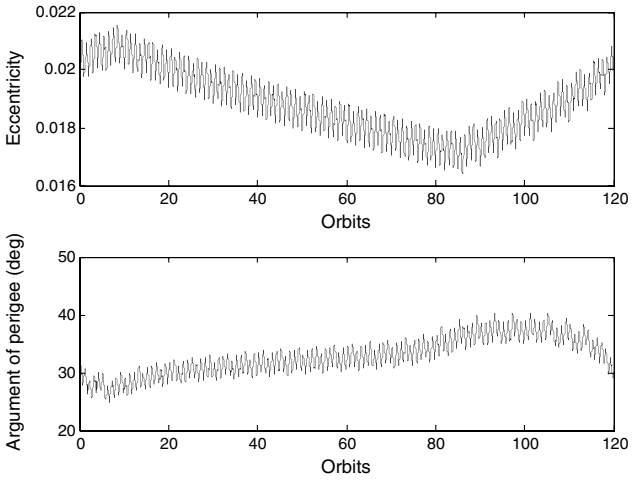

Fig. 12 Orbit eccentricity and argument of perigee during minimum time inclination change with hanging tether, showing propagated solutions.

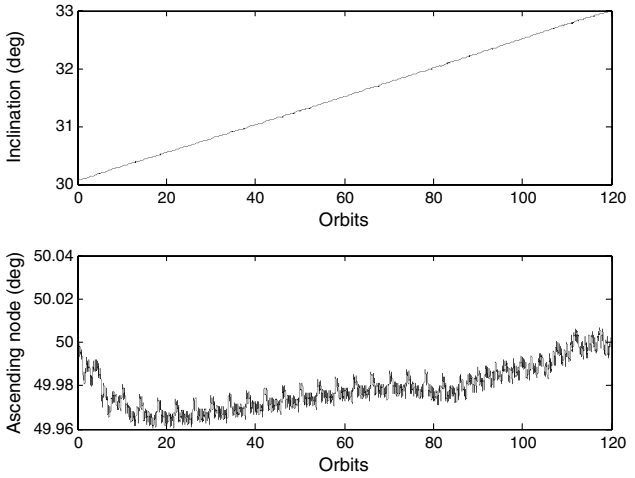

Fig. 13 Orbit inclination and right ascension of ascending node during minimum time orbit boost with hanging tether, showing propagated solutions.

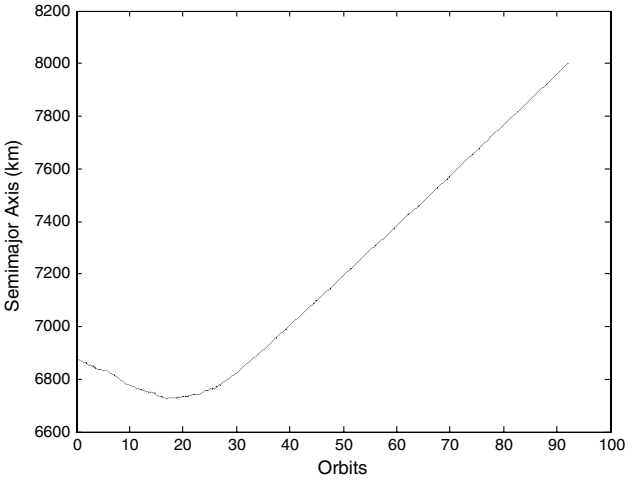

Fig. 14 Orbit semimajor axis during minimum time orbit boost with spinning tether, showing propagated solution.

Minimum Time Orbit Boost with Spinning Tether

In this section, an orbit boost is considered with a spinning electrodynamic tether instead of a hanging tether. The problem is to maneuver the electrodynamic tether system defined in the previous section from the starting orbit

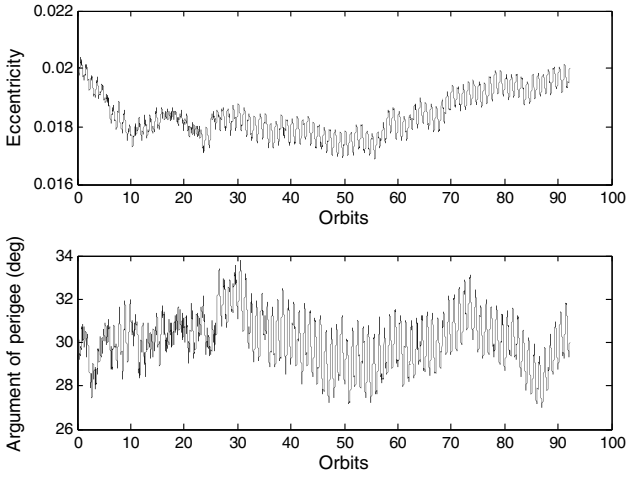

Fig. 15 Orbit eccentricity and argument of perigee during minimum time orbit boost with spinning tether, showing propagated solutions.

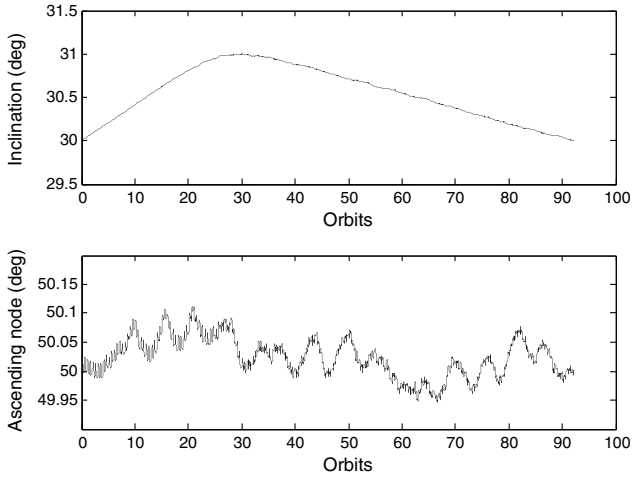

Fig. 16 Orbit inclination and right ascension of ascending node during minimum time orbit boost with spinning tether, showing propagated solutions.

$$a = 6878 \text{ km}, \quad e = 0.02, \quad \omega = 30 \text{ deg}, \quad i = 30 \text{ deg}$$
$$\Omega = 50 \text{ deg}, \quad \nu = 0 \tag{52}$$

to the final orbit

$$a = 8000 \text{ km}, \quad e = 0.02, \quad \omega = 30 \text{ deg}, \quad i = 30 \text{ deg}$$
$$\Omega = 50 \text{ deg} \tag{53}$$

in minimum time, with the tether spinning such that $\theta = 3t$, where t is represents the mean anomaly of a circular orbit at 6878 km. In other words, the system spins at a constant rate of approximately three times per orbit. The problem was solved using a 3:1 discretization, with $N_{\omega_1} = 20$, and the time domain divided into 30 subintervals. The minimum time for the maneuver was found to be 92.17 orbits, which is slightly less than that required for a hanging tether. Figure 14 shows the variation in the semimajor axis during the maneuver, Fig. 15 shows the eccentricity and argument of perigee, and Fig. 16 shows the inclination and right ascension of the ascending node. The maneuver dynamics are similar in principle to those of a hanging tether, except that the system descends quicker, achieving the initial change in inclination faster. Unlike the hanging tether, the current must be phased properly with the tether direction. Hence, the electric current is bang–bang throughout the maneuver. The propagated results show that good accuracy is still maintained.

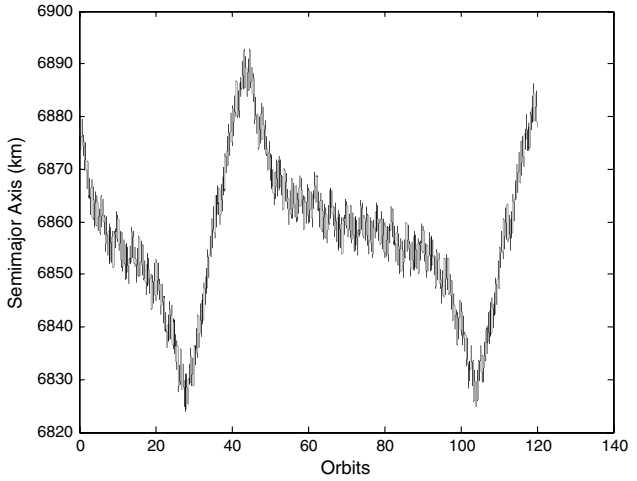

Fig. 17 Orbit semimajor axis during minimum time orbit boost with spinning tether, showing propagated solution.

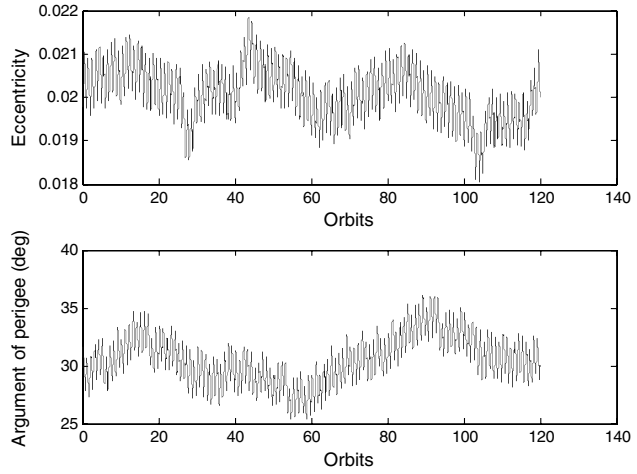

Fig. 18 Orbit eccentricity and argument of perigee during minimum time orbit boost with spinning tether, showing propagated solutions.

Minimum Time Inclination Change with Spinning Tether

In this final problem, the advantage of using a spinning electrodynamic tether for changing orbit inclination is illustrated. The problem is to maneuver the electrodynamic tether system defined in the previous section from the starting orbit

$$a = 6878 \text{ km}, \quad e = 0.02, \quad \omega = 30 \text{ deg}, \quad i = 30 \text{ deg}$$
$$\Omega = 50 \text{ deg}, \quad \nu = 0 \tag{54}$$

to the final orbit

$$a = 6878 \text{ km}, \quad e = 0.02, \quad \omega = 30 \text{ deg}$$
$$i = 34.5 \text{ deg}, \quad \Omega = 50 \text{ deg} \tag{55}$$

in minimum time. This represents an increase in the inclination of 4.5 deg, which is 50% greater than the change in inclination considered earlier with a hanging tether. The problem was solved using a 3:1 discretization, with $N_{\omega_1} = 20$, and the time domain divided into 30 subintervals. The minimum time for the maneuver was found to be 120.05 orbits, which is approximately equal to the time required to maneuver the hanging tether with a change of only 3 deg in inclination. Hence, the spinning system is much more efficient at changing the inclination. This is consistent with previous suboptimal results [10]. Figure 17 shows the variation in the semimajor axis during the maneuver, Fig. 18 shows the eccentricity and argument of perigee, and Fig. 19 shows the inclination and right ascension of the ascending

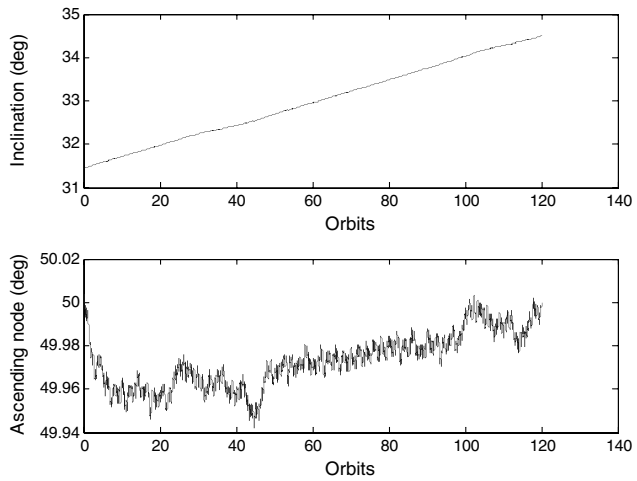

Fig. 19 Orbit inclination and right ascension of ascending node during minimum time orbit boost with spinning tether, showing propagated solutions.

node. These results show that the semimajor axis varies over a wider range compared with the hanging tether maneuver. In contrast, the other orbital elements are slightly more constrained due to the averaging effect of using a spinning tether.

Conclusions

The discretization technique proposed in this paper takes advantage of the best features of the traditional pseudospectral method, combined with quadrature integration rules, for approximating the dynamics of multiple-timescale systems. The resultant smoothing of the slow-state dynamics results in significantly fewer optimization variables than a full transcription of the original problem, but without a significant sacrifice in accuracy. In the main case of an electrodynamic tether, trajectories can be optimized over long time intervals using a high number of nodes to capture the bang–bang variation in electric current typical of many optimal maneuvers. Fewer nodes are used to approximate the state trajectories, which retain the information about the switches in current due to the use of numerical integration rules. No analytic integration or simplifications of the dynamical equations are necessary. When used to optimize the trajectory of a spinning electrodynamic tether system, faster maneuvers are possible than can be obtained with a hanging/librating tether. The results of a specific example show that, after 120 orbits, a spinning tether system can achieve a 4.5 deg increase in inclination compared with a 3 deg increase for a hanging tether system.

Appendix: Derivation of Integration Matrix

We aim to derive the entries of the integration matrix

$$\mathcal{I}_{j-1,k} \triangleq \int_{-1}^{\tau_j} \phi_k(\tau)\,\mathrm{d}\tau, \qquad j = 1,\ldots,N_{\omega_1}; \qquad k = 0,\ldots,N_{\omega_2} \tag{A1}$$

The general expression for the Lagrange interpolating polynomial is

$$\phi_k(\tau) = \prod_{\substack{j=0\\ j\neq k}}^{N_{\omega_2}} \left(\frac{\tau-\tau_j}{\tau_k-\tau_j}\right) = \frac{g(\tau)}{(\tau-\tau_k)g'(\tau_k)}, \qquad k = 0,\ldots,N_{\omega_2} \tag{A2}$$

By definition of the CGL nodes,

$$g(\tau) = (\tau^2-1)T'_N(\tau) = (N/2)[T_{N+1}(\tau) - T_{N-1}(\tau)] \tag{A3}$$

Hence, we have the following:

$$g'(\tau) = (N/2)[T'_{N+1}(\tau) - T'_{N-1}(\tau)] \tag{A4}$$

The Christoffel–Darboux identity for Chebyshev polynomials can be written as

$$B_m(\tau,z) = \sum_{k=0}^{m} 2T_k(\tau)T_k(z) = \frac{T_{m+1}(\tau)T_m(z) - T_m(\tau)T_{m+1}(z)}{\tau - z} \tag{A5}$$

Using this relationship, we obtain the following:

$$\begin{aligned} B_N(\tau,z) + B_{N-1}(\tau,z) &= \frac{T_{N+1}(\tau)T_N(z) - T_N(\tau)T_{N+1}(z)}{\tau - z} \\ &\quad + \frac{T_N(\tau)T_{N-1}(z) - T_{N-1}(\tau)T_N(z)}{\tau - z} \\ &= \frac{2}{N}\left[\frac{g(\tau)T_N(z) - T_N(\tau)g(z)}{\tau - z}\right] \end{aligned} \tag{A6}$$

Let $z = \tau_k$, where τ_k is a zero of $g(\tau)$,

$$B_N(\tau,\tau_k) + B_{N-1}(\tau,\tau_k) = \frac{2}{N}\left[\frac{g(\tau)T_N(\tau_k)}{\tau - \tau_k}\right] \tag{A7}$$

It is evident that the right-hand side of Eq. (A7) resembles the form of the Lagrange interpolating polynomial that needs to be integrated to form the entries of the integration matrix in Eq. (A1). Integrating both sides of Eq. (A7) leads to

$$\int_{-1}^{\tau_j} [B_N(\tau,\tau_k) + B_{N-1}(\tau,\tau_k)]\,\mathrm{d}\tau = \frac{2}{N} g'(\tau_k)T_N(\tau_k)\mathcal{I}_{j-1,k} \tag{A8}$$

Using Eqs. (A4) and (A5) and rearranging, we obtain

$$\begin{aligned} \mathcal{I}_{j-1,k} &= \frac{T_N(\tau_k)}{[T'_{N+1}(\tau_k) - T'_{N-1}(\tau_k)]} \int_{-1}^{\tau_j} \left[\sum_{p=0}^{N} 2T_p(\tau)T_p(\tau_k)\right. \\ &\quad \left. + \sum_{p=0}^{N-1} 2T_p(\tau)T_p(\tau_k)\right] \mathrm{d}\tau \end{aligned} \tag{A9}$$

The integral of a Chebyshev polynomial may be evaluated as

$$\int_{-1}^{\tau_j} T_p(\tau)\,\mathrm{d}\tau = \frac{1}{2}\left[\frac{T_{p+1}(\tau)}{p+1} - \frac{T_{p-1}(\tau)}{p-1}\right]_{-1}^{\tau_j} \tag{A10}$$

References

[1] Bryson, A. E., Desai, M. N., and Hoffman, W. C., "The Energy-State Approximation in Performance Estimation of Supersonic Aircraft," *Journal of Aircraft*, Vol. 6, 1969, pp. 481–487. doi:10.2514/3.44093

[2] Lu, P., and Pierson, B. L., "Optimal Aircraft Terrain-Following Analysis and Trajectory Generation," *Journal of Guidance, Control, and Dynamics*, Vol. 18, No. 3, 1995, pp. 555–560. doi:10.2514/3.21422

[3] Williams, P., "Three-Dimensional Aircraft Terrain-Following via Real-Time Optimal Control," *Journal of Guidance, Control, and Dynamics*, Vol. 30, No. 4, 2007, pp. 1201–1206. doi:10.2514/1.29145

[4] Ross, I. M., Gong, Q., and Sekhavat, P., "Low-Thrust, High-Accuracy Trajectory Optimization," *Journal of Guidance, Control, and Dynamics*, Vol. 30, No. 4, July–Aug. 2007, pp. 921–933. doi:10.2514/1.23181

[5] Ross, I. M., Sekhavat, P., Fleming, A., and Gong, Q., "Optimal Feedback Control: Foundations, Examples, and Experimental Results for a New Approach," *Journal of Guidance, Control, and Dynamics*, Vol. 31, No. 2, 2008, pp. 307–321. doi:10.2514/1.29532

[6] Desai, P. N., and Conway, B. A., "Two-Timescale Discretization Scheme for Collocation," *Journal of Guidance, Control, and Dynamics*, Vol. 31, No. 5, 2008, pp. 1316–1322. doi:10.2514/1.33974

[7] Herman, A. L., and Conway, B. A., "Direct Optimization Using Collocation Based on High-Order Gauss–Lobatto Quadrature Rules," *Journal of Guidance, Control, and Dynamics*, Vol. 19, No. 3, 1996, pp. 592–599. doi:10.2514/3.21662

[8] Williams, P., "Optimal Orbital Transfer with Electrodynamic Tether," *Journal of Guidance, Control, and Dynamics*, Vol. 28, No. 2, 2005, pp. 369–371. doi:10.2514/1.12016

[9] Tragesser, S. G., and San, H., "Orbital Maneuvering with Electrodynamic Tethers," *Journal of Guidance, Control, and Dynamics*, Vol. 26, No. 5, 2003, pp. 805–810. doi:10.2514/2.5115

[10] Williams, P., "Simple Approach to Orbital Control Using Spinning Electrodynamic Tethers," *Journal of Spacecraft and Rockets*, Vol. 43, No. 1, 2006, pp. 253–256. doi:10.2514/1.16608

[11] Stevens, R., and Wiesel, W., "Large Time Scale Optimal Control of an Electrodynamic Tether Satellite," *Journal of Guidance, Control, and Dynamics*, Vol. 31, No. 6, 2008, pp. 1716–1727. doi:10.2514/1.34897

[12] Williams, P., Tragesser, S., and Ockels, W., "Orbital Maneuvering with Librating and Spinning Electrodynamic Tethers," American Astronautical Society Paper 09-243, Feb. 2009.

[13] Williams, P., "Hermite–Legendre–Gauss–Lobatto Direct Transcription Methods in Trajectory Optimization," *Journal of Guidance, Control, and Dynamics*, Vol. 32, No. 4, 2009, pp. 1392–1395. doi:10.2514/1.42731

[14] Elnagar, G., Kazemi, M. A., and Razzaghi, M., "The Legendre Pseudospectral Method for Discretizing Optimal Control Problems," *IEEE Transactions on Automatic Control*, Vol. 40, No. 10, 1995,

pp. 1793–1796.
doi:10.1109/9.467672

[15] Ross, I. M., and Fahroo, F., *Legendre Pseudospectral Approximations of Optimal Control Problems*, Vol. 295, Lecture Notes in Control and Information Sciences, Springer, New York, 2003, pp. 327–342.

[16] Williams, P., "Jacobi Pseudospectral Method for Solving Optimal Control Problems," *Journal of Guidance, Control, and Dynamics*, Vol. 27, No. 2, 2004, pp. 293–297.
doi:10.2514/1.4063

[17] Elnagar, G., and Kazemi, M. A., "Pseudospectral Chebyshev Optimal Control of Constrained Nonlinear Dynamical Systems," *Computational Optimization and Applications*, Vol. 11, 1998, pp. 195–217.
doi:10.1023/A:1018694111831

[18] Fahroo, F., and Ross, I. M., "Direct Trajectory Optimization by a Chebyshev Pseudospectral Method," *Journal of Guidance, Control, and Dynamics*, Vol. 25, No. 1, 2002, pp. 160–166.
doi:10.2514/2.4862

[19] Williams, P., "A Gauss–Lobatto Quadrature Approach for Solving Optimal Control Problems," *The Australian & New Zealand Industrial and Applied Mathematics Journal*, Vol. 47, July 2006, pp. C101–C115.

[20] Williams, P., and Trivailo, P., "Optimal Parameter Estimation of Dynamical Systems Using Direct Transcription Methods," *Inverse Problems in Science and Engineering*, Vol. 13, No. 4, 2005, pp. 377–409.
doi:10.1080/17415970500104499

[21] Ross, I. M., and Fahroo, F., "Pseudospectral Knotting Methods for Solving Optimal Control Problems," *Journal of Guidance, Control, and Dynamics*, Vol. 27, No. 3, 2004, pp. 397–405.
doi:10.2514/1.3426

[22] Gill, P. E., Murray, W., and Saunders, M. A., "SNOPT: An SQP Algorithm for Large-Scale Constrained Optimization," *SIAM Journal on Optimization*, Vol. 12, No. 4, 2002, pp. 979–1006.
doi:10.1137/S1052623499350013

[23] Beletsky, V. V., and Levin, E. M., "Dynamics of Space Tether Systems," *Advances in the Astronautical Sciences*, Vol. 83, Univelt, Inc., San Diego, CA, 1993.